16th Australasian Fluid Mechanics Conference
Crown Plaza, Gold Coast, Australia
2-7 December 2007

Development of Casbar: a Two-phase Flow Code for the Interior Ballistics Problem

R. J. Gollan[1], I. A. Johnston[2], B. T. O'Flaherty[1] and P. A. Jacobs[1]

[1]Division of Mechanical Engineering
The University of Queensland, Brisbane, Queensland, AUSTRALIA

[2]Weapons Systems Division
Defence Science and Technology Organisation, Edinburgh, South Australia, AUSTRALIA

Abstract

Accurate modelling of gun interior ballistic processes aids in the design and analysis of guns and their propelling charges. Presently, the most accurate modelling of the interior ballistics problem is provided by two-phase, multidimensional computational fluid dynamics (CFD) codes.

We present our development of a CFD code, `Casbar`, which solves a two-phase (gas/particulate) flow problem in axisymmetric geometries. Our model is based on the governing equations for two-phase flow derived from separated flow theory. A finite-volume discretisation of the governing equations is used. The resulting set of equations is solved with a timestep-splitting approach based on the separation of various physical processes. We also present the modelling for the component physics such as propellant combustion and interphase drag. In addition, the solver includes the motion of the projectile and its influence on the flow dynamics. The capabilities of the code are demonstrated with some verification exercises.

Introduction

The design of high-performance guns can be assisted by a complement of experimental and numerical investigative techniques. The numerical simulation of the interior ballistic process is desirable for a number of reasons: simulations provide data that cannot be directly measured by experiment; numerical investigation of design parameters is simpler and less costly than physical experimentation; and simulations can be safely performed at conditions that might risk gun damage or catastrophic failure in an actual experiment. However, a crucial aspect of numerical simulations is ensuring their validity in modelling the real-world process. In this paper, we look at the development and implementation of such a model which simulates an interior ballistic process based on a two-phase flow model for axiymmetric gun geometries.

Tha basic interior ballistic process may be considered as a heat engine: solid propellant, providing a source of chemical energy, is burnt and eventually converted to kinetic energy of the projectile [8]. The analysis is complicated by the interacting physical processes that occur during the ballistic cycle. The sequence of these processes is as follows. The ballistic cycle begins with an igniter venting hot gases and particulates into the gun chamber. These igniter products initiate combustion of the solid propellant through a process of heat transfer to the propellant surface. The combustion process of the solid propellant releases more gas which raises the pressure in the chamber. In some cases, not all of the solid propellant is ignited simultaneously and as such an ignition flame will spread through the propellant bed. Once combustion of the propellant has commenced, chamber pressurisation accelerates because the propellant's linear burn rate typically increases with pressure and, in the case of progessive propellant grains, the available surface area for burning is also increasing. Once the 'shot start' pressure is achieved the projectile begins to travel down-bore, and the resultant volume increase and work done on the projectile start to moderate the chamber pressurisation. The challenge for the numerical model is to capture these effects in an accurate manner to conduct meaningful calculations of the gun performance.

The existing codes available for gun simulations can be broadly classified into two types: (1) lumped-parameter codes and (2) CFD-type codes. Lumped-parameter codes have been successfully used to simulate a range of gun systems with reasonable accuracy, and are particularly useful for conducting quick design calculations and for use as an aid during live gun firing experiments [3]. A defined pressure distribution between gun breech and projectile base is assumed (typically Lagrangian pressure distribution, or a modified form thereof), and the propellant is approximated as combusting uniformly and having an even distribution throughout the barrel. Lumped-parameter models do not perform well when the physical system deviates substantially from a one-dimensional approximation, and are not able to capture important processes such as pressure wave development. CFD-type codes belong to the present generation of simulation tools and have a better capability to represent the flow that arises in complex gun geometries. A CFD code allows for the treatment of details of the physical setup which are not possible in a lumped-parameter model, such as location of the igniter and nonuniformities in flamespreading. We restrict our attention to CFD-type modelling for the remainder of the paper.

Simulation of the interior ballistics problem requires the selection of an appropriate mathematical model. The question of an appropriate model is hotly contested in the literature, and as Gokhale and Krier [9] state, "a unified and universally acceptable description of such a complex flow is not expected and probably will never be satisfactorily achieved in the future." There are numerous governing models for the gun problem but most are just a variation on one of two themes: (1) separated flow theory and (2) continuum mixture theory. Separated flow theory is based on a formal averaging technique applied over the two (separated) flows of gas and particulates devised by Anderson and Jackson [4]. The idea in continuum mixture theory is to treat the gas/particulate flow as one continuum flow of a mixture and extract the behaviour of the component phases. The treatment of multi-phase flows in this way can be traced back to Truesdell [20]. Despite the differences in modelling philosophy, the form of the resulting two-phase flow equations does not differ greatly between the two theories — there are some additional inertial "coupling terms" present in the formulation based on continuum mixture theory. Gokhale and Krier [9] have shown that the differing formulations have no practical significance on flow field calculations in the interior ballistics problem, at least for their specific problem. In this code development work, we have adopted a model, based on separated flow theory, provided by Gough and Zwarts [11].

Description of the model

Governing equations

The equations for conservation of mass, momentum and energy of the various phases are presented below without derivation. There is no energy equation for the particulate phase as the model assumes an incompressible and isothermal particulate phase. The full derivation which uses a formal averaging technique applied to the separated continuum flows may be found in the article by Gough and Zwarts [11]. In two dimensions, the integral form of the conservation system is

$$\frac{d}{dt}\int_\Omega U\,dV + \frac{1}{\Omega}\int_S F\,dy - \frac{1}{\Omega}\int_S G\,dx = Q \qquad (1)$$

where the vector of conserved quantities U, flux vectors in the x- and y-direction F and G, and the source vector Q, are

$$U = \begin{bmatrix} \varepsilon_g\rho_g \\ \varepsilon_g\rho_g u_g \\ \varepsilon_g\rho_g v_g \\ \varepsilon_g\rho_g E \\ \varepsilon_p\rho_p \\ \varepsilon_p\rho_p u_p \\ \varepsilon_p\rho_p v_p \end{bmatrix},$$

$$F = \begin{bmatrix} \varepsilon_g\rho_g u_g \\ \varepsilon_g\left(\rho_g u_g^2 + p\right) \\ \varepsilon_g\rho_g v_g u_g \\ \varepsilon_g\left(\rho_g E u_g + p u_g\right) \\ \varepsilon_p\rho_p u_p \\ \varepsilon_p\left(\rho_p u_p^2 + \tau_p\right) \\ \varepsilon_p\rho_p v_p u_p \end{bmatrix}, \quad G = \begin{bmatrix} \varepsilon_g\rho_g v_g \\ \varepsilon_g\rho_g u_g v_g \\ \varepsilon_g\left(\rho_g v_g^2 + p\right) \\ \varepsilon_g\left(\rho_g E v_g + p v_g\right) \\ \varepsilon_p\rho_p v_p \\ \varepsilon_p\rho_p u_p v_p \\ \varepsilon_p\left(\rho_p v_p^2 + \tau_p\right) \end{bmatrix},$$

$$Q = \begin{bmatrix} \dot{m} \\ \dot{m}u_p - (\vec{F}_d)_x + p\frac{\partial\varepsilon_g}{\partial x} \\ \dot{m}v_p - (\vec{F}_d)_y + p\frac{\partial\varepsilon_g}{\partial y} \\ -\left|\vec{F}_d\right|\left|\vec{u_p}\right| + \dot{m}\left[e_{\text{chem}} + \frac{1}{2}\vec{u_p}\cdot\vec{u_p}\right] \\ -\dot{m} \\ -\dot{m}u_p + (\vec{F}_d)_x \\ -\dot{m}v_p + (\vec{F}_d)_y \end{bmatrix}.$$

While not shown here, the mass conservation equations are further expanded to incorporate multiple gas species and solid types. A brief nomenclature follows in tabular form.

Symbols

Ω	control volume, m^3
S	control surface, m^2
ε	porosity, volume fraction
ρ	density, kg/m^3
u	velocity in the x-direction (axial), m/s
v	velocity in the y-direction (radial), m/s
E	total energy $(E = e + \frac{1}{2}(u+v)^2)$, J
e	internal energy, J
p	gas pressure, Pa
τ_p	'pressure' on particulate phase $(\tau_p = R + p)$, Pa
R	intergranular stress, Pa
$\dot{m}$	rate of gas mass generation due to propellant combustion, kg/s
$\vec{F}_d$	interphase drag, N
e_{chem}	chemical energy of gaseous products due to propellant combustion, J/kg

Subscripts

g	related to gas phase
p	related to particulate (solid) phase

Assumptions of the model

The assumptions of separated flow theory as applied to the interior ballistics problem are stated clearly and concisely by Gokhale and Krier and are reproduced here (see p.9, Ref. [9]):

1. The two phases are interdispersed but separate; coupled by appropriate interaction terms which account for heat, momentum and mass transport between the phases.
2. Each phase is a separate continuum with unique substantial derivatives.
3. The total cross-sectional area is the sum of gas and solid flow areas.
4. The solid particles are large compared to molecules and hence will not contribute to the total pressure of the mixture.
5. The solid is considered as a pseudo-fluid.
6. The solid (propellant) burning results in loss of mass from the solid phase and equivalent gain by the gas phase.
7. The gases are inviscid except for their action on the particles through the drag. The gas viscosity is assumed to be known as a function of temperature.
8. Heat transfer to the particles due to conduction and radiation is neglected. (In `Casbar` local gas temperature is used as the combustion trigger.)
9. The diameter of the particle is an average diameter of all the particles at that location.

Most models based on separated flow theory treat the solid phase as incompressible. If that is the case, an energy conservation equation is not required for the solid phase. As there is no energy equation for the solid phase, the heat transfer between the gas and solid is computed based on some assumed temperature distribution within the solid particles (usually a cubic function). In `Casbar`, no heat transfer is computed — the local gas temperature is used as an ignition criteria. Baer and Nunziato [5] note that the incompressible solid assumption limits the applicability of the model to situations of low-pressure gas generation. Low-pressure is defined here as a pressure resulting in no significant compression or distortion of the solid particles.

The formal averaging used to derive the equations of separated flow theory are based on a volume size which is large enough to contain many particles but small in comparsion to the dimensions of the system. When this constraint is met, the averaging is independent of the exact nature of the weighting function. The idea of an averaging volume is central to separated flow theory. Some argue that the use of this volume-averaged model places a lower limit on the size of the computational mesh. Beyond some lower limit, the assumption of containing many particles is violated and the averaged equations are no longer valid [14]. In practice, we have not found any difficulties with small mesh sizes and this view is held by others [1].

Numerical solution procedure

The governing equations are discretised in a finite-volume manner on a regular mesh of quadrilateral cells. The procedure uses

[1] Personal communication with Mr Clive Woodley, QinetiQ, Fort Halstead

explicit time-marching from a set of initial conditions to compute a time-accurate solution. The various physical processes are timestep-split with the update procedure over one complete timestep being:

```
update_due_to_ignition(dt)
update_due_to_gas_transport(dt)
update_due_to_particulate_transport(dt)
update_due_to_projectile_motion(dt)
update_due_to_general_source_terms(dt)
update_due_to_grain_combustion(dt)
```

The treatment of the gas transport, particulate transport and integration of source terms is second-order in time using a predictor-corrector method. The spatial reconstruction and flux calculation is based on the work used in the code `mb_cns`[12]. The present code, `Casbar` (Collaborative Australian Ballistics Research code), is a two-phase extension of the single-phase code `mb_cns`. In the work presented here, all calculations have made use of the AUSMDV flux calculator [21]. The general source terms include all source terms in the vector Q that are not explicitly treated elsewhere. The effects of igntion modelling and grain combustion are handled as a separate update process as this is convenient from a code implementation perspective.

Modelling of physics subprocesses

The various physical processes of importance in the interior ballistics problem each require the implementation of a model describing the behaviour.

Grain combustion, $\dot{m}$.
If the local gas temperature exceeds a defined ignition threshold, then combustion of the solid propellant and gas generation are assumed to occur. More advanced ignition modelling, based on propellant grain heating, will be considered for inclusion in subsequent code development. The rate of solid surface regression, $\dot{r}$, is related to the gas production by

$$\dot{m} = \varepsilon_p \rho_p \frac{S_p(r)}{V_p(r)} \dot{r} \tag{2}$$

where S_p is the combined surface area of the propellant grains in a given finite volume, and V_p is the combined volume of the grains in that same finite volume. The value for V_p is calculated directly from $V_p = \varepsilon_p V$ where V is the volume of the finite-volume cell. In the implementation, look-up tables containing grain mass, volume, and surface area as a function of regression distance r are pre-computed from exact, analytical form-functions of grain geometry. A range of common grain geometries, including 7- and 19-perforated cylinders, and grains layered with different propellant materials, are currently supported. The use of look-up tables speeds computation, and mass conservation is maintained over each timestep by interpolating quantities at both $r(t)$ and $r(t+dt) = r(t) + \dot{r}\,dt$. The rate of surface regression, $\dot{r}$, also called the propellant linear burning rate, is modelled by Vielle's law,

$$\dot{r} = A + Bp^n \tag{3}$$

where A, B and n are constants for a given propellant material. Multiple parameter sets are used across pressure ranges to maintain accuracy, if need be.

Gas equation of state.
Due to the high densities of gas generated during propellant combustion, the real gas behaviour of the gas mixture needs to be considered. The Noble-Abel equation can be used to account for the finite amount of volume occupied by the high-density collection of gas particles.

$$\rho = \frac{p}{(RT + bp)} \tag{4}$$

where b is the co-volume for the gas and R is the specific gas constant in this context. For a mixture of Noble-Abel gases, the co-volume value for the mixture is computed based on a mole-weighted average of the component co-volumes. Further details about the equation of state and its implementation for this project work are given in the report by Johnston [13].

Intergranular stress, R, and wave speed, a_p.
The intergranular stress is a measure of the particle-to-particle force in the packed propellant bed. In this work, the rheological model as used by Gough and Zwarts [11] has been adopted:

$$R = \rho_p a_1^2 \varepsilon_0^2 \left(\frac{1}{\varepsilon_g} - \frac{1}{\varepsilon_0} \right) \tag{5}$$

where a_1 and ε_0 are empirical constants. Based on this stress model, there is a related equation for the speed of propagation of small disturbances (wave speed) in the granular bed:

$$a_p = \begin{cases} a_1(\varepsilon_0/\varepsilon_g) & \varepsilon_g \leqslant \varepsilon_0 \\ a_1 \exp[-\kappa(\varepsilon - \varepsilon_0)] & \varepsilon_0 < \varepsilon_g < \varepsilon_* \\ 0 & \varepsilon_g \geqslant \varepsilon_* \end{cases} \tag{6}$$

where κ and ε_* are again emprical constants. The stress attenuation is accounted for with the factor κ, and ε_* represents the porosity value above which granular wave speed is zero.

Interphase drag, $\vec{F}_d$.
The interphase drag appears in the momentum equations for both the gas and particulate phases, and the gas phase energy equation. It is a momentum sink in the gas phase and a corresponding source of momentum for the solid phase, consistent with Newton's third law. The accuracy of the calculated drag force is limited by the experimental data available for correlation. Most of the data available is for a packed bed, at steady-state and low Reynolds number. In the course of the interior ballistics cycle, the particulate bed becomes fluidized, the flow field is transient and there are regions of high Reynolds number beyond the range of experimental data. This means that the correlations for drag force must be used with some caution. Gokhale and Krier [9] provide a more thorough discussion about the complexities of drag force calculation.

For our purposes, we choose a model for drag force calculation that appeared in the work by Gough and Zwarts [11] and is based on the relation by Ergun [7].

$$\vec{F}_d = \frac{\varepsilon_p}{D_e} \left| \vec{u_g} - \vec{u_p} \right| \left(\vec{u_g} - \vec{u_p} \right) \rho_g \phi \tag{7}$$

where D_e is the effective diameter taken as $D_e = \frac{6V}{S}$ based on the current volume and surface area of the grain and ϕ is used to include the effect of bed fluidization.

$$\phi = \begin{cases} 1.75 & \varepsilon_g \leqslant \varepsilon_0 \\ 1.75 \left[\frac{1-\varepsilon_g}{1-\varepsilon_0} \frac{\varepsilon_0}{\varepsilon_g} \right]^{0.45} & \varepsilon_0 < \varepsilon_g \leqslant \varepsilon_l \\ 0.3 & \varepsilon_l < \varepsilon_g \leqslant 1 \end{cases} \tag{8}$$

Projectile motion. The projectile motion is modelled in the (east-west) axial dimension only and is included in the flow simulations using the Cartesian cut-cell method for moving bodies [24]. The volumes of the cut-cells V_i are allowed to vary

as $\frac{1}{2} < \bar{V}_i < \frac{3}{2}$, normalised by the volume of the underlying grid cell. The projectile's influence on the flow is treated by applying a moving wall boundary condition. The pressure and intergranular stress at the moving wall interface is taken as equal to the neighbouring cell values.

The projectile dynamics are updated according to Newton's second law, $F = m\ddot{x}$. The applied force is composed of the gas pressure, integranular stress and an effective resistance pressure, p_r, exerted on the projectile. Thus

$$F = \begin{cases} 0 & p_r \geq |p_w - p_e|, \\ \left(p_w - p_e - \hat{\dot{x}} p_r(x)\right) A_p & \text{otherwise} \end{cases} \tag{9}$$

where the pressure terms on the west piston face (p_w) and east face (p_e) include gas pressure and intergranular stress, $p = \varepsilon_g p_g + \varepsilon_p (p_g + R)$ and the effective resistance pressure p_r is linearly interpolated between set values located along the bore. Multiplication by the unit vector for x-velocity of the projectile, $\hat{\dot{x}}$, gives the correct direction for the resistive force.

In the case of a rifled bore, the inertia of the projectile is increased by a rotational component as the projectile 'spins up'. We treat this as an effective mass in Newton's second law, and it may be calculated as

$$\begin{aligned} F &= m_{eff}\ddot{x} \\ &= \left(m + \tfrac{4\pi^2 I}{n^2 D^2}\right)\ddot{x} \end{aligned} \tag{10}$$

where the moment of inertia of a rigid body $I = m{k_{zz}}^2$, the radius of gyration about the z-axis for a solid cylinder $k_{zz} = \frac{\sqrt{2}}{4}D$ and n is the number of turns per calibre.

Verification exercises

As part of the verification process for the code, a number of test cases have been computed. It is important to try to select test cases which exercise isolated components of the code so as to reduce the complexity during the development phase. Table 1 dislays a selection of tests that have been performed using `Casbar` and describes which parts of the modelling it exercises. We discuss four particular verification tests in detail: (1) the treatment of arbitrary source terms; (2) a constant speed projectile moving through gas; (3) a projectile moving under the influence of a pressure differential; and (4) a complete one-dimensional gun (AGARD gun [2]).

Treatment of arbitrary source terms

In this verification exercise, the timestep-splitting of gas flow and source term integration is tested. The test case is the computation of a gas flow field in one-dimension with arbitrary source terms. The source terms are chosen such that an analytical solution to the Euler equations may be found for the system. This type of test case was first proposed by Clarke [6] and expanded on in the work by Lowe and Clarke [16]. Clarke [6] argued that because of the complexity involved in the full interior ballistics process, "there is clearly every motivation to look for simpler models, that isolate key elements in the process, and illuminate important physical features." In this test, the key elements of gas phase flow, source term integration and the implementaton of the timestep-splitting method are verified. By judicious selection of source terms — selecting sources to give mass and energy generation — the system approximates the type of flow field in the interior of a gun.

The system of governing equations for the verification test describes the flow of an inviscid compressible gas with perfect behaviour:

$$U_t + F_x(U) = S(U)$$

where the vectors, U, F_x and S are

$$U = \begin{bmatrix} \rho \\ \rho u \\ \rho E \end{bmatrix}, \quad F_x(U) = \begin{bmatrix} \rho u \\ \rho u^2 + p \\ \rho u(E + pv) \end{bmatrix}, \quad S(U) = \begin{bmatrix} G \\ F \\ H \end{bmatrix}$$

The sources are chosen to be:

$$\begin{aligned} G &= \frac{\rho \tilde{G}}{a} \\ F &= (Na + u)\frac{\rho \tilde{G}}{a} \\ H &= (Nua + pv + E)\frac{\rho \tilde{G}}{a} \end{aligned}$$

The particular conditions chosen for this test correspond to the example provided in Section 6.1 of the article by Lowe and Clarke [16]. The calculations are performed on the domain $[-0.5, 0.5]$ m. The inputs for the test case are given in Table 2.

Variable	Value
$\tilde{G}$	1294301 kg/m^{3}s
N	0.1
γ	1.4
p_0	10140 Pa
a_0	330.34 m/s
u_0	0.0 m/s

Table 2: Inputs and initial conditions for the Euler flow with source terms

The simulations were performed on three grids of different resolution to ensure grid independence: 100 cells in the x-direction, 200 cells and 500 cells. As the code is inherently two-dimensional there are 2 cells in the y-direction despite the fact that the problem itself is one-dimensional. The coarsest grid calculations took approximately 0.7 s to simulate 1.9 ms of flow, while the finest grid took 32.3 s. These simulations were performed on a single process thread of a dual-core Intel Xeon chip (2.00 GHz).

The results of the simulation are shown in Figure 1 where the velocity field and sound speed field are compared to the analytical solution. The analytical solution is given in the article by Lowe and Clarke [16] and additional details are provided in the report by Clarke [6]. For clarity, the results of the simulation using 100 cells are shown. The usual problems of shock smearing in a shock-capturing method are evident at $t = 1.1$ ms and $x \approx 0.48$ m. The numerical solution agrees well with the analytical solution and this gives confidence in certain aspects of the code implementation, namely, the calculation of gas transport, the integration of source terms and the timestep-splitting approach for separation of operators.

Projectile and flow interaction

The interaction between the projectile and the flow domain was verified with two tests. The first tested the effect of the projectile on the domain when moving at a constant velocity. The second tested the effect of the projectile on the domain when accelerating under a pressure difference. No rifling, resistance or heat loss was included in either case such that an analytical solution could be used for comparison.

Constant-speed projectile.
The first test case was performed on a grid of 100×20 cells of dimensions $[0,1] \times [0, 0.2]$ m with reflecting boundary conditions. It was filled initially with quiescent perfect air at

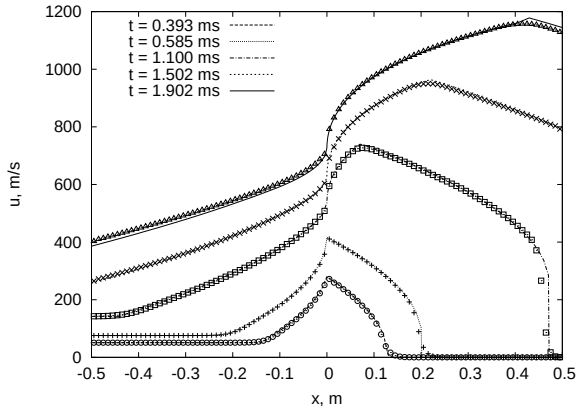

(a) velocity field

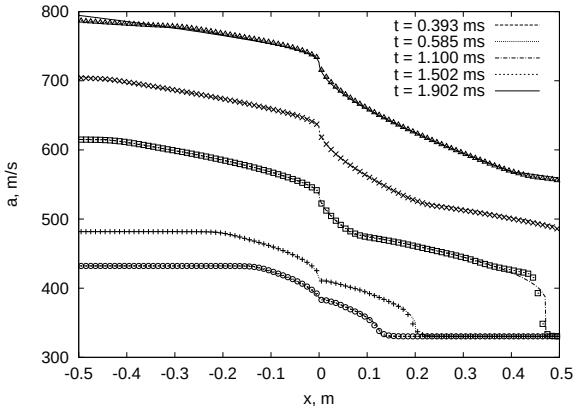

(b) sound speed field

Figure 1: Inviscid compressible flow with sources: a comparison of numerical and analytical solutions. The lines represent the analytical solution and the symbols represent the numerical solution. The numerical solution was computed with 100 cells in the x-direction.

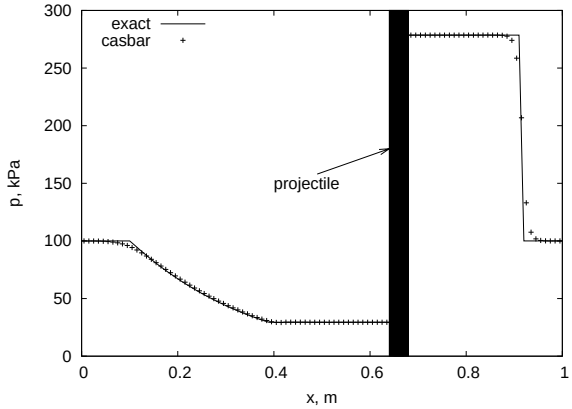

(a) pressure profile

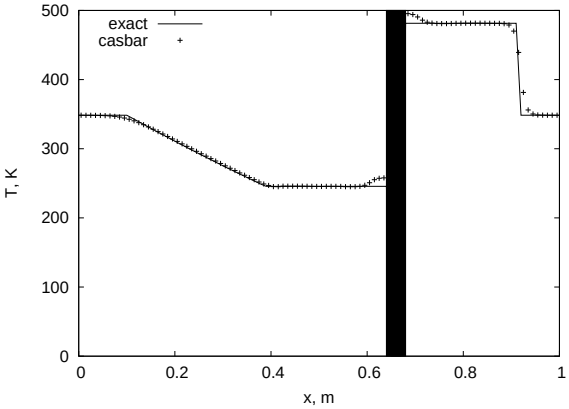

(c) temperature profile

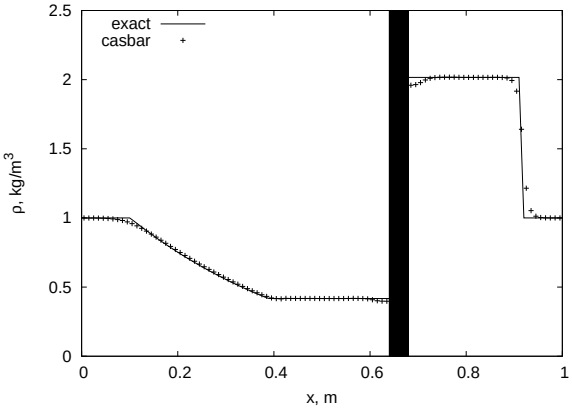

(b) density profile

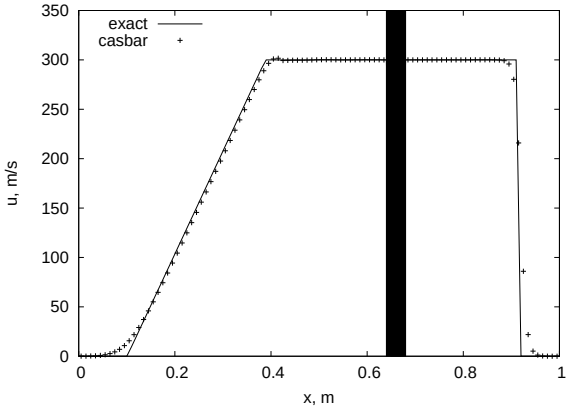

(d) x-velocity profile

Figure 2: Constant velocity projectile with u = 300 m/s to the right.

Test description	Components tested	References
Closed vessel	Coupling of flow solver and grain combustion module	
Sod shock tube	Gas transport	Sod [18]
Treatment of arbitrary source terms	Timestep-splitting method	Clarke [6]/Lowe and Clarke [16]
Gas flow with porosity discontinuity	Treatment of "nozzling" terms	Lowe [15]
Constant-speed projectile	Coupling of flow and projectile motion	
Pressure driven projectile	Coupling of flow and projectile motion	AGARD Group [1]
AGARD gun	Complete coupling, all components tested	AGARD Group [2]

Table 1: Verification exercises for various aspects of the `Casbar` implementation.

$\rho = 1\,\mathrm{kg/m^3}$ and $p = 100\,\mathrm{kPa}$. The piston was of dimensions $[0.4, 0.44] \times [0, 0.2]$ and moves at a constant velocity of $(u, v) = (300, 0)$ m/s. Profiles of pressure, temperature, density and x-velocity were taken from the line $y = 0.1$ m after $800\,\mu$s and compared to the analytical solution derived from wave theory. The numerical values are in excellent agreement with the analytical values except at the projectile boundary as shown in Figure 2. We believe this discrepancy arises from a limitation in the Cartesian cut-cell method but we choose not to speculate any further at the present. In general, this case demonstrates the correct implementation of the moving wall boundary condition because its bulk effect on the flow, in terms of driven shock and expansion waves, are correctly computed.

Pressure-driven projectile.
For the unsteady isentropic flow of an ideal gas in a gun with an infinitely long reservoir, the relationships for projectile position and time as a function of velocity [1] are

$$\bar{t} = \frac{2}{\gamma+1}\left\{\left[1-\left(\frac{\gamma-1}{2}\right)\bar{u}_p\right]^{-(\gamma+1)/(\gamma-1)} - 1\right\} \quad (11)$$

$$\bar{x}_p = \frac{2}{\gamma-1}\left\{1+\bar{t}-\left[1+\left(\frac{\gamma+1}{2}\right)\bar{t}\right]^{2/(\gamma+1)}\right\} \quad (12)$$

where the dimensionless forms of time, position and velocity are

$$\bar{t} = \frac{p_0 A t}{m_p a_0}\ ,\ \bar{x}_p = \frac{p_0 A x_p}{m_p a_0^2} \text{ and } \bar{u}_p = \frac{u_p}{a_0}.$$

Here, p_0 is the reservoir pressure, a_0 is the speed of sound in the reservoir gas, γ is the ratio of specific heats, A is the cross-sectional area of the gun, u_p is the projectile velocity and x_p is the projectile position.

The second test case was performed on a grid of 100×20 of dimensions $[-10, 10] \times [0, 0.2]$m with transmissive boundary conditions. The left half is initially filled with quiescent perfect air at $\rho = 1\,\mathrm{kg/m^3}$ and $p = 100\,\mathrm{kPa}$ whereas the right half is a near vacuum ($p = 1.0 \times 10^{-10}$ Pa — a perfect vacuum causes difficulty in a numerical computation). The projectile was of dimensions $[-1.0, 1.0] \times [0, 0.2]$ m, mass 1 kg and initially at rest. A plot of non-dimensional velocity as a function of non-dimensional time for both the numerical and analytical solution is shown in Figure 3. This figure shows that the calculation of pressure forces on the projectile faces and the projectile dynamics are correctly implemented in the code.

AGARD gun

The "AGARD gun" is based on a test case defined in AGARD Advisory Report No.172 [2]. It has become something of a standard test case among the interior ballistics modelling community. The test case is completely fictitious and does not physically correspond to any particular gun configuration. We consider this test case as part of the verification process because

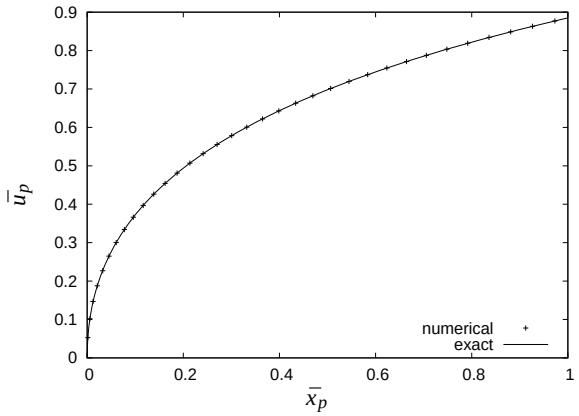

Figure 3: Accelerating a 1kg projectile under a 100kPa pressure difference

it provides a weak form of verification in the form of code-by-code comparison. In contrast, we consider the process of validation as the more complex task of assessing how well the code models reality by comparison to experimental data.

The details of the test case are completely specified in the aforementioned report [2]. Some of the essential features of the gun are: a calibre of 132 mm; propellant mass of 9.5255 kg; 7-perforation cylindrical propellant grains; chamber length of 762 mm; total gun length of 5080 mm; projectile mass of 45.359 kg; and a constant projectile resistance pressure of 13.79 MPa. The test case specifies a one-dimensional and a two-dimensional version of the case, which is related to how the initial igniter material is injected into the domain. We have chosen to use our axisymmetric code (ie. two-dimensional) to simulate the one-dimensional case so as to directly compare against other results made available to us.

The simulations of the gun were performed on three grids as listed in Table 3. The settling porosity, ε_0, which appears in the models for intergranular stress and interphase drag was taken as equal to the initial bed porosity, $\varepsilon = 0.4211$. A constant intergranular wave speed of 254 m/s as specified in the test case was used which means that Equation 6 was not actually used in this calculation. The simulation included a mixture of three gases: the propellant gas, the ambient air and the igniter gas.

The results for this test case are usually reported in terms of muzzle velocity, maximum pressures at the breech and projectile base, and shot exit time. These quantities are reported in Table 3. The values compare favourably with the results reported by others (see Table 3), such as Toro [19] and Nussbaum et al. [17]. Figure 4 shows four plots from the simulations on the finest grid: pressure at breech; pressure at projectile base; projectile displacement; and projectile velocity. The calculations from other codes are shown also, namely, XKTC [10],

CTA1 [23] and FHIBS [22]. Pressure waves corresponding to breech ignition are observed, as expected. Some noise, manifested as high-frequency, low magnitude oscillations, appears in the results. It is easiest to see in the base pressure curve just after peak pressure, and has been identified as a behaviour inherent to the Cartesian cut-cell methodology employed. Current and future work looks to address this issue of noise, but it does not presently affect the usefulness of the code for simulations of ballistic performance.

Conclusion

We have described a model for two-phase flow appropriate for the internal ballistics problem and its component models for the physical subprocesses. Our code, `Casbar`, implements a finite-volume method to solve the governing set of equations for the conservation of mass, momentum and energy. The code has been verified on a number of test cases which aim to isolate various components of the modelling.

The future direction for this work will address validation of the code — assessing how well the tool models reality by comparison to experimental data. Aditionally, we plan to investigate the use of more sophisticated flow field reconstruction techniques to alleviate the 'noise' that is observed as part of the Cartesian cut-cell method.

Acknowledgements

We would like to thank Mr Clive Woodley, QinetiQ, for kindly providing us with the results from the CTA1 and FHIBS simulations of the AGARD gun, and for giving his permission to use those results here.

References

[1] AGARD, Ballistic–range technology, AGARDograph 138, North Atlantic Treaty Organisation, 1970.

[2] AGARD, Fluid dynamics aspects of internal ballistics, AGARD Advisory Report 172, North Atlantic Treaty Organisation, 1982.

[3] Anderson, R. and Fickie, K., IBHVG2 — a user's guide, BRL-TR-2829, Ballistic Research Laboratory, Aberdeen Proving Ground, 1987.

[4] Anderson, T. and Jackson, R., A fluid mechanical description of fluidized beds - equations of motion, *Industrial and Chemical Engineering Fundamentals*, **6**, 1967, 527–539.

[5] Baer, M. and Nunziato, J., A two–phase mixture theory for the deflagration-to-detonation transition (DDT) in reactive granular materials, *International Journal of Multiphase Flow*, **12**, 1986, 861–889.

[6] Clarke, J., Compressible flow produced by distributed sources of mass: An exact solution, COA Report 8710, College of Aeronautics, Cranfield Institute of Technology, 1987.

[7] Ergun, S., Fluid flow through packed columns, *Chemical Engineering Progress*, **48**, 1952, 89–94.

[8] Freedman, E., *Gun Propulsion Technology*, AIAA, 1988 .

[9] Gokhale, S. and Krier, H., Modeling of unsteady two-phase reactive flow in porous beds of propellant, *Progress in Energy and Combustion Science*, **8**, 1982, 1–39.

[10] Gough, P., The XNOVAKTC code, PGA-TR-86-1, Ballistic Research Laboratory, Aberdeen Proving Ground, 1986.

[11] Gough, P. and Zwarts, F., Modelling heterogeneous two-phase reacting flow, *AIAA Journal*, **17**, 1979, 17–25.

[12] Jacobs, P., MB_CNS: A computer program for the simulation of transient compressible flows, Departmental Report 10/96, Department of Mechanical Engineering, The University of Queensland, 1996.

[13] Johnston, I., The Noble–Abel equation of state: Thermodynamic derivations for ballistics modelling, Technical Report DSTO-TN-0670, Defence Science and Technology Organisation, 2005.

[14] Lowe, C., *CFD Modelling of Solid Propellant Ignition*, Ph.D. thesis, College of Aeronautics, Cranfield University, 1996.

[15] Lowe, C., Two-phase shock-tube problems and numerical methods of solution, *Journal of Computational Physics*, **204**, 2005, 598–632.

[16] Lowe, C. and Clarke, J., A class of exact solutions for the euler equations with sources: Part I, *Mathematical and Computer Modelling*, **36**, 2002, 275–291.

[17] Nussbaum, J., Helluy, P., Hérard, J.-M. and Carrière, A., Numerical simulations of gas-particulate flows with combustion, *Flow, Turbulence and Combustion*, **76**, 2006, 403–417.

[18] Sod, G., Survey of several finite difference methods for systems of nonlinear hyperbolic conservation laws, *Journal of Computational Physics*, **26**, 1978, 1–31.

[19] Toro, E., *Riemann-problem-based Techniques for Computing Reactive Two-phase Flows*, Springer-Verlag, 1989, volume 351, Numerical Combustion of *Lecture Notes in Physics* 472–481.

[20] Truesdell, C., *Rational Thermodynamics*, McGraw-Hill, New York, 1969.

[21] Wada, Y. and Liou, M.-S., An accurate and robust flux splitting scheme for shock and contact discontinuities, *SIAM Journal of Scientific Computing*, **18**, 1997, 633–657.

[22] Woodley, C., Billett, S., Lowe, C., Speares, W. and Toro, E., The FHIBS internal ballistics code, in *22nd International Symposium on Ballistics*, Vancouver, 2005.

[23] Woodley, C., Carrière, A., Franco, P., Gröger, T., Hensel, D., Nussbaum, J., Kelzenberg, S. and Longuet, B., Comparisons of internal ballistics simulations of the AGARD gun, in *22nd International Symposium on Ballistics*, Vancouver, 2005.

[24] Yang, G., Causon, D., Ingram, D., Saunders, R. and Batten, P., A cartesian cut cell method for compressible flows Part B: moving body problems, *The Aeronautical Journal*, **101**, 1997, 57–62.

Grid resolution axial × radial	Maximum breech pressure MPa	Maximum base pressure MPa	Muzzle velocity m/s	Shot exit time ms
46 × 6	404	378	704	14.59
86 × 9	401	377	686	14.15
125 × 18	393	371	672	13.91
Results by others				
XKTC	352	–	668	15.51
CTA1 [23]	385	361	687	14.94
FHIBS [22]	385	356	686	15.03
Toro [19]	–	–	≈ 700	≈14
Nussbaum et al. [17]	377	344	694	15.75

Table 3: Summary of results for simulation of the AGARD gun at various grid resolutions and comparison to other reported results.

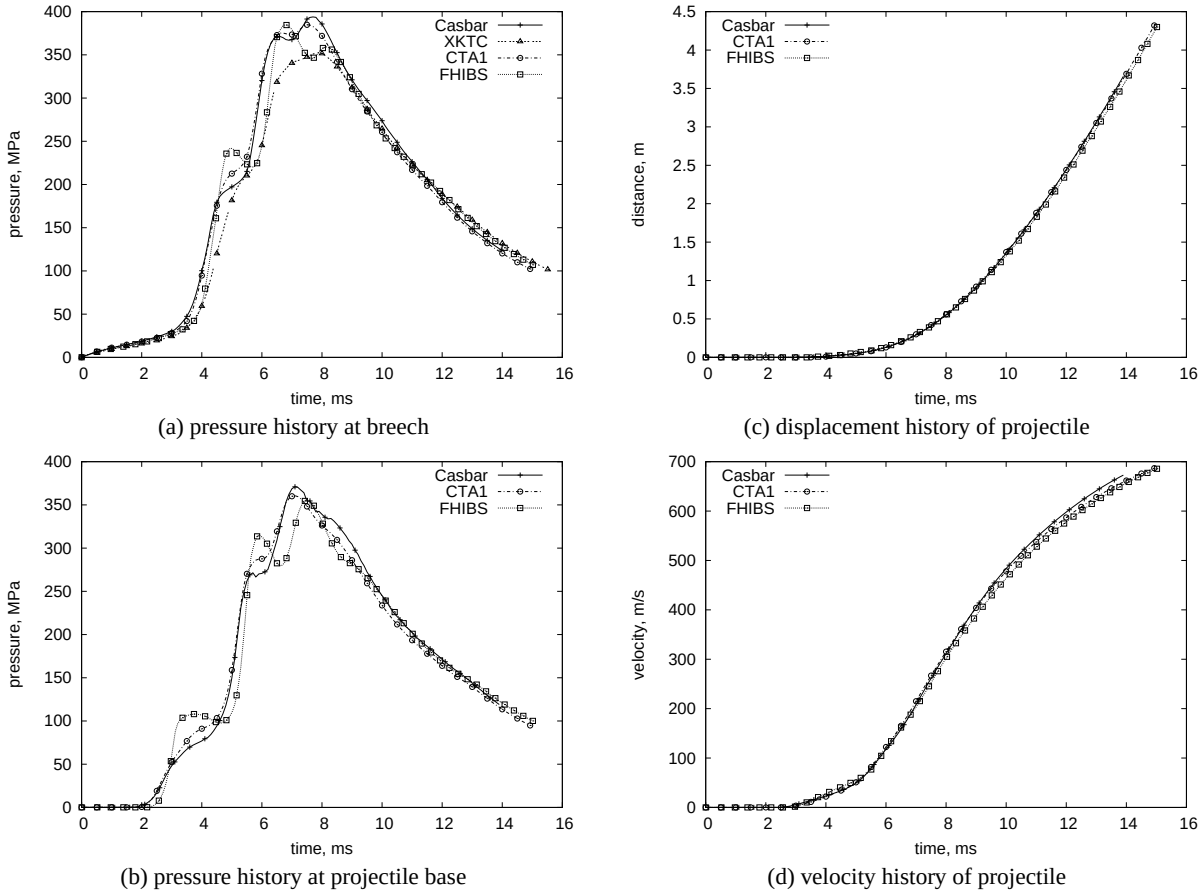

(a) pressure history at breech

(c) displacement history of projectile

(b) pressure history at projectile base

(d) velocity history of projectile

Figure 4: Simulation of the AGARD gun test case. Results are shown for the finest grid resolution for the `Casbar` simulations.